Raman spectroscopy and dielectric measurements of betaine rubidium iodide dihydrate

2002 J. Phys.: Condens. Matter 14 4553

(http://iopscience.iop.org/0953-8984/14/17/326)

INSTITUTE OF PHYSICS PUBLISHING JOURNAL OF PHYSICS: CONDENSED MATTER

J. Phys.: Condens. Matter **14** (2002) 4553–4565 PII: S0953-8984(02)32949-7

Raman spectroscopy and dielectric measurements of betaine rubidium iodide dihydrate

A Almeida[1], M R Chaves[1], Pedro Teles[1], Filipa Pinto[1], A Klöpperpieper[2] and João Amaral[1]

[1] Departamento de Física, IFIMUP, CFUP, Faculdade de Ciências da Universidade do Porto, Rua do Campo Alegre 687, 4169-007 Porto, Portugal
[2] Fachbereich Physik, Universität des Saarlandes, 66041 Saarbrüken, Germany

Received 23 January 2002, in final form 15 March 2002
Published 18 April 2002
Online at stacks.iop.org/JPhysCM/14/4553

Abstract

Dielectric measurements and Raman spectroscopy have shown for betaine rubidium iodide dihydrate, with formula $[(CH_3)_3N^+CH_2COO^-]_2RbI{\cdot}2H_2O$, BRbI for short, the existence of two phase transitions in this compound, PT_1 (at $T_{c1} = 190$ K) and PT_2 (at $T_{c2} = 90$ K). The former phase transition is related to the loss of translational and librational degrees of freedom of water molecules and this, as shown by dielectric data, triggers a relaxation process leading to a complete 'freezing in' of protons within the unit cell, and therefore, producing a proton-glass state.

1. Introduction

Interesting results on a new family of hydrates having the general formula $[(CH_3)_3N^+CH_2COO^-]_nXY{\cdot}2H_2O$ ($n = 1, 2$; X = K; Y = Br, I) were reported recently [1, 2]. Although all members of this family exhibit phase transitions involving a freezing process of water molecules, each compound reveals its own peculiarities. In fact, for $n = 1$, X = K and Y = Br (BKBr) the two water molecules are involved in several sorts of asymmetric hydrogen bond, O–H···Br and O–H···O, while for $n = 2$, X = K and Y = I (BKI) [3, 4] the system of water molecules is involved in zigzag chains in the planes nearly perpendicular to the c-axis of the unit cell.

A new compound with $n = 2$, X = Rb and Y = I (BRbI) was grown from an aqueous solution. The analysis of the crystal structure of this material shows that it is isomorphic with that of BKI, both exhibiting the lowest symmetry among this family of betaine compounds, triclinic with space group C_i^1 ($P\bar{1}$) at room temperature [1, 5]. Some disorder in the rotational degrees of water molecule reorientations was also found at this temperature [5].

In spite of the similarity between the structural properties of BKI and BRbI, some differences in the phase transition sequence for the two compounds, studied by means of Raman scattering and dielectric dispersion, were found. There is evidence for the existence of a

proton-glass state at low temperatures in BRbI, and this behaviour resembles the transition from dynamic to static disorder, exhibited by $Cs_5H_3(SO_4)_4{\cdot}H_2O$ [6, 7]. This is an interesting result because, in general, proton-glass states are found in mixed compounds due to the coexistence of antiferroelectric and ferroelectric interactions.

In some hydrates, at high temperatures, water molecules are dynamically disordered, the protons being exposed to double-well-shaped potentials. With lowering temperature, protons in these compounds may form a disordered pattern, randomly occupying the minima of these wells. This process can also happen in other compounds containing hydrogen bonds [8–12]. Dominated by electric dipole interactions, these asymmetric units have analogies with some of the spin-glass features and are designated as pseudo-spins. Some properties of these proton glasses were tentatively described by Ising models where random bonds and random fields are the main interactions [10, 12, 13].

The study of the electric current versus the temperature in BRbI, under a dc field of 760 V cm^{-1}, between 290 and 190 K has shown the existence of electrical conductivity above $T_{c1} = 190$ K. At high temperatures, protons have enough energy to 'jump' over the potential barriers in the zigzag chain of water molecules, producing in this way a protonic current by means of a hopping process.

2. Experimental details

The crystals of BRbI were cut in the form of carefully oriented and optically polished rectangular parallelepipeds, $4 \times 3 \times 3$ mm^3, with the X-axes perpendicular to the (110) planes, Y parallel to $[\bar{1}10]$ and Z parallel to [001]. The crystallographic axes were determined with an accuracy of $\pm 1^\circ$ by means of x-ray diffraction.

The complex dielectric constant was measured in the X-, Y- and Z-directions, with an automatic HP 4192A LCR meter, as a function of temperature in the 20–300 K interval and in the frequency range 10 kHz–13 MHz, under an ac electric field of 1 V cm^{-1}. Heating and cooling runs were performed at the rate of 0.3 K min^{-1}. The polarization reversal was studied at different fixed temperatures with a modified Sawyer–Tower circuit, driven at the frequency of 0.5 Hz. The pyroelectric current was measured at the temperature rate of 1 K min^{-1}, with a standard short circuit [14] at zero dc field and under several different values of dc fields.

Raman spectra were obtained using the polarized light of an Ar^+ laser, Coherent INNOVA 90 ($\lambda = 514.5$ nm), in a right-angle scattering geometry. The scattered light was analysed using a Jobin-Yvon T64000 spectrometer equipped with a CCD and a photon-counting detector. The spectral slit width was about 1.5 cm^{-1}. The samples were placed in a closed-cycle helium cryostat with a temperature stability of about ± 0.2 K. The temperature was measured with a silicon diode attached to the sample holder. The actual sample temperatures were estimated to differ by less than 1 K from the temperature readings. Temperature homogeneity in the sample was achieved with a copper mask set-up.

3. Electric measurements

3.1. Dielectric constant

The temperature dependences of the real and imaginary parts of the complex dielectric constant in the frequency region 10 kHz–13 MHz, for the X- and Y-directions, are depicted in figure 1. In the Z-direction, BRbI presents a much weaker induced polarization, and therefore it will not be considered here. In both X- and Y-directions, we can observe some anomalies for $\varepsilon'(T)$ and $\varepsilon''(T)$ around $T_{c1} \simeq 190$ K, that signal a phase transition (PT_1). This phase transition is

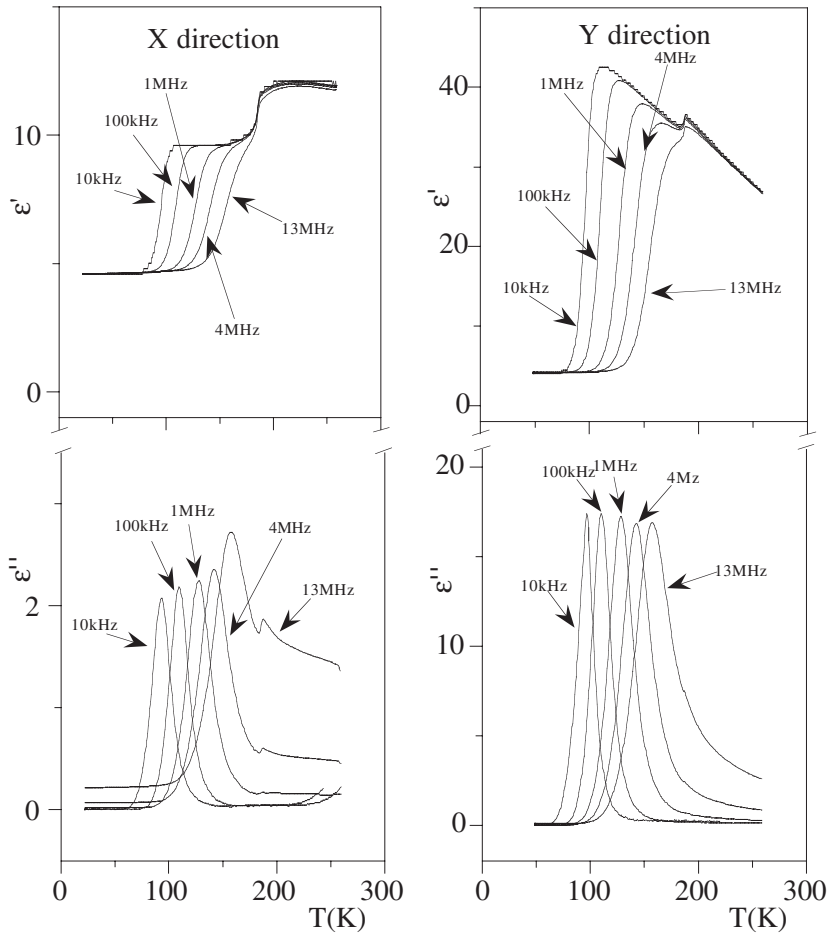

Figure 1. Temperature dependences of the complex dielectric constant along X- and Y-directions at different frequencies in the 10 kHz–13 MHz range.

followed by a highly dispersive peak in $\varepsilon''(T)$, and by an abrupt decrease in $\varepsilon'(T)$, that are associated with another phase transition (PT_2) at $T_{c2} \simeq 90$ K. These two phase transitions occur at well-determined temperatures, and are related to relaxation processes of different nature.

The experimental data referred to were fitted with a Cole–Cole function [15]:

$$\varepsilon^* = \varepsilon'(\omega) - \mathrm{i}\varepsilon''(\omega) = \varepsilon(\infty) + \frac{\Delta\varepsilon}{1 + (\mathrm{i}\omega/\omega_r)^\beta} \tag{1}$$

where $\varepsilon(\infty)$, ω_r and β are adjustable parameters. The analysis of the relaxation's dynamical mechanisms by the latter fitting procedure revealed two very different relaxation processes separated by PT_1. The logarithm of the relaxation frequency obtained, $\omega_r(T)$, is depicted in figure 2. In order to estimate the activation energy (E_a) of the relaxation process of order–disorder type, below PT_1, we have fitted these frequencies with a usual Arrhenius law: $\omega_r = \omega_0 \exp(-E_a/k_B T)$ and with a Vogel–Fulcher (VF) law: $\omega_r = \omega_0 \exp(-E_a/k_B(T - T_{VF}))$, where k_B is Boltzmann's constant.

The best results were obtained with the Arrhenius fit and the following adjustable parameters were attained: $\omega_0 = 6.89 \times 10^{11}$ Hz, $E_a = 0.15 \pm 0.01$ eV. We could not

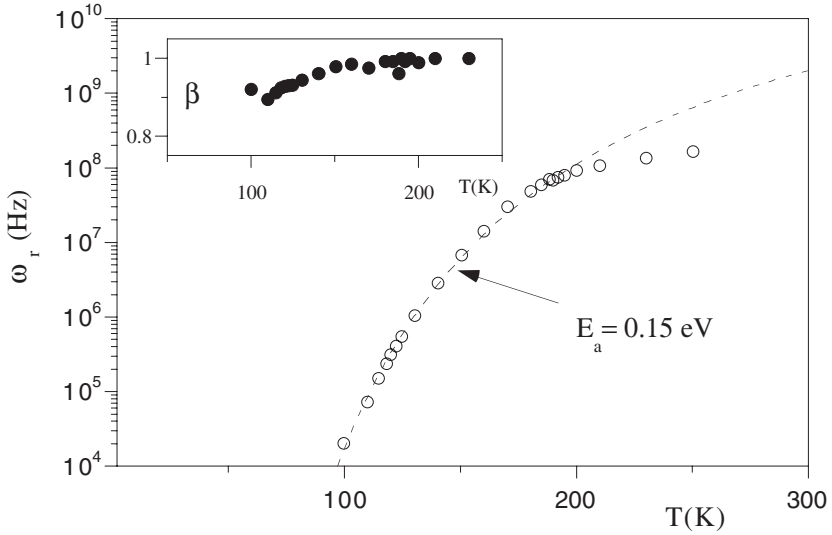

Figure 2. A semilogarithmic plot of the relaxation frequency ω_r versus the temperature and respective Arrhenius law fit. The inset shows the temperature evolution of the dispersion coefficient β.

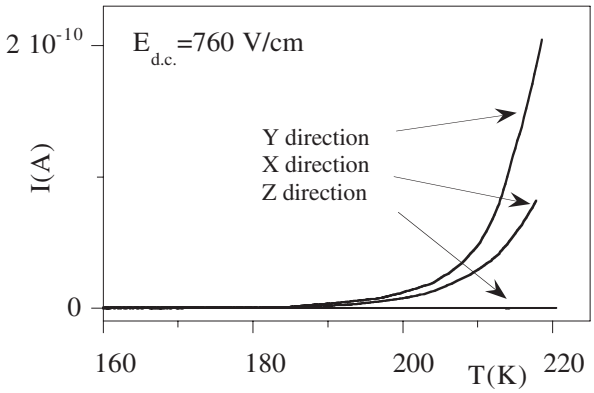

Figure 3. Electric currents measured along X-, Y- and Z-directions in the temperature range 160–230 K for a dc electric field of 760 V cm^{-1}.

estimate the activation energy above 190 K with acceptable accuracy, due to the low number of existing data points above this temperature. However, there is clear evidence for completely different behaviours of the relaxation frequency $\omega_r(T)$ above and below 190 K. The dispersive coefficient obtained, $\beta(T)$, is very close to unity above T_{c1}, although it slightly decreases below this temperature, reaching 0.89 at T_{c2}, as can be seen in the inset of figure 2. The β-values indicate very clearly a polydispersive character in this material below T_{c1}.

3.2. Electric current measurements

Above T_{c1}, the dc electric currents $I(T)$ measured in the X- and Y-directions under a dc field of 760 V cm^{-1} show very intense signals, significantly increasing with increasing temperature, as can be seen in figure 3. This behaviour is very probably due to protonic conduction that then gradually disappears below T_{c1}.

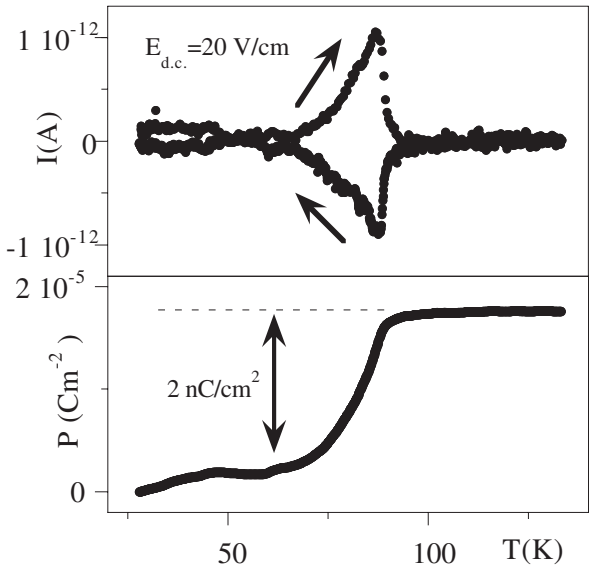

Figure 4. Temperature evolution of the electric current (I) under a dc electric field of 20 V cm^{-1}, measured along the Y-direction in the temperature range 20–140 K, and respective integrated polarization (P).

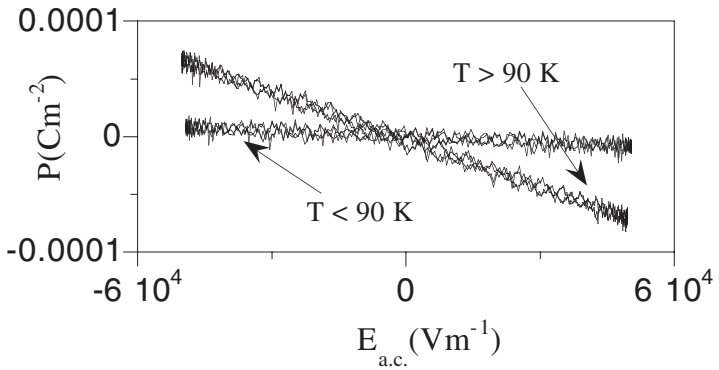

Figure 5. Induced polarization in BRbI as a function of an ac electric field, measured along the Y-direction, at 0.5 Hz, for $T > 90$ K and $T < 90$ K.

No pyroelectric current was detected at zero field, in the temperature range studied (290–10 K). However, under a dc field of 20 V cm^{-1}, one can observe an anomaly in the electric current $I(T)$ at approximately 90 K (figure 4), that corresponds to a shift in the induced polarization of about 2 nC cm^{-2}. This induced polarization becomes quite negligible below this temperature, i.e., <1 nC cm^{-2}.

Neither simple nor double hysteresis loops have been observed in the temperature range studied, excluding the possibility of ferroelectric or antiferroelectric behaviour of BRbI. With increasing temperature, there is a sudden increase of the slope of the straight lines $P(E)$ at $T_{c2} = 90$ K, proving that below this temperature it becomes very difficult to induce any polarization in the sample (figure 5).

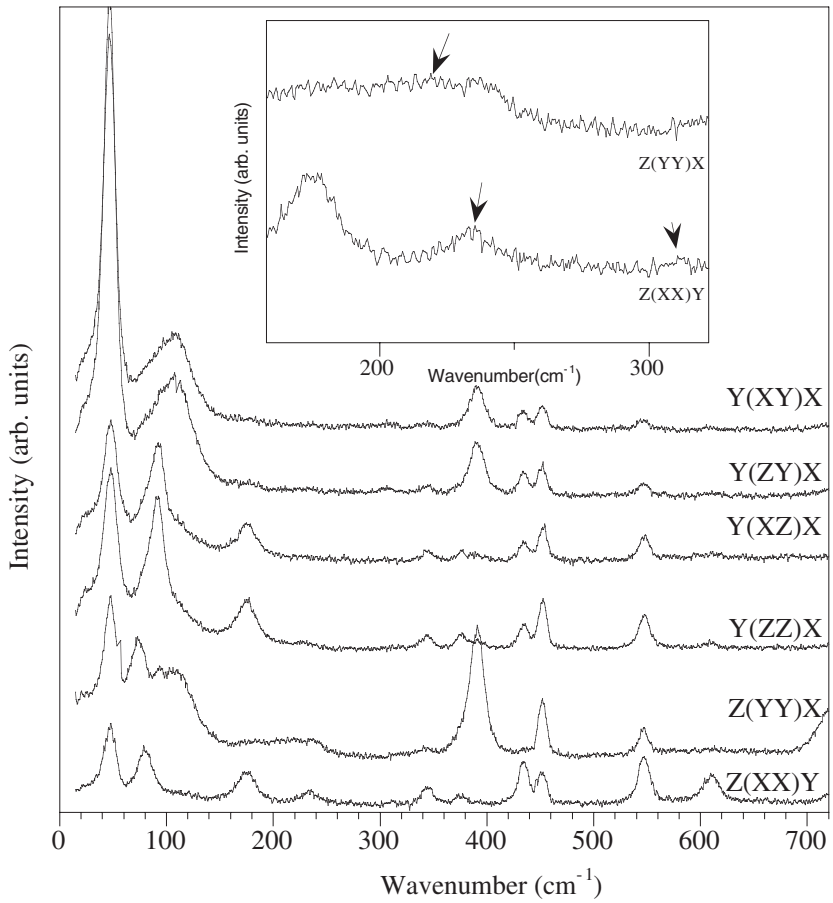

Figure 6. Low-frequency Raman spectra of BRbI for six different geometries. The inset shows weak lines in $Z(YY)X$ (upper spectrum) and $Z(XX)Y$ (lower spectrum) geometries.

4. Raman spectra

According to the x-ray diffraction results at room temperature [5], the primitive cell of BRbI contains one formula unit ($Z = 1$). Both I and Rb ions occupy special positions of C_i symmetry, while all atoms of betaine ions and water molecules are in C_1 positions. The vibrational spectra of the crystal lattice, in terms of 135 IR- or Raman-active optical and three acoustic phonon modes, are

$$\Gamma_{\text{crystal}} = (66A_g + 69A_u)_{\text{opt}} + 3(A_u)_{\text{ac}}; \qquad \Gamma_{\text{tr}}(\text{Rb}) = \Gamma_{\text{tr}}(\text{I}) = 3A_u;$$
$$\Gamma_{\text{ext}}(2H_2O) = \Gamma_{\text{ext}}(2\text{betaine}) = (3A_g + 3A_u)_{\text{tr}} + (3A_g + 3A_u)_{\text{lib}};$$
$$\Gamma_{\text{int}}(2H_2O) = 3A_g + 3A_u; \qquad \Gamma_{\text{int}}(2\text{betaine}) = 51A_g + 51A_u;$$

where the subscripts ‘ext’, ‘tr’, ‘lib’ and ‘int’ denote, respectively, external, translation, libration and internal modes.

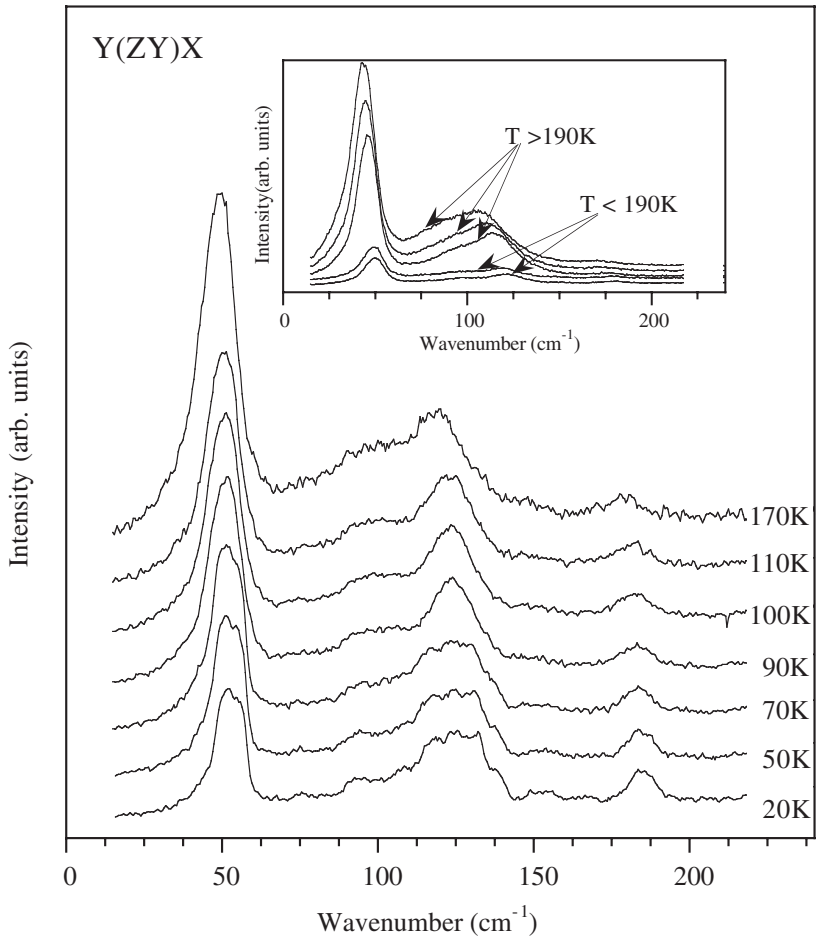

Figure 7. Temperature evolution of Raman spectra of BRbI in the $Y(ZY)X$ scattering geometry, below 190 K, in the 15–220 cm^{-1} frequency region. The inset shows the temperature evolution of the same spectra, above and below 190 K.

4.1. External modes

Raman spectra in the region 15–700 cm^{-1} at room temperature (RT) are shown in figure 6 in several different geometries. As the crystal possesses triclinic symmetry, all scattering geometries represent phonons of A_g symmetry and contain equivalent information. Six modes are expected in the low-frequency spectra, at room temperature, corresponding to betaine external modes: from factor group analysis no Raman-active external modes are expected from either I or Rb ions [3]. At room temperature, water molecules are dynamically disordered [5] and therefore their librational and translational modes are expected to be rather weak and overdamped. Two modes at 218 and 234 cm^{-1} are observed in the inset of figure 6, in $Z(YY)X$ and $Z(XX)Y$ geometries, and can be assigned to water translations. There is no direct evidence for the existence of librational modes (a broader, weaker mode appears around 310 cm^{-1}, and might be considered as a water libration mode, although apparently this mode might also represent CH_3 torsion of betaine molecules [3]). This indicates a rather weak bond of the water molecules to the crystal lattice (weak Rb–OH_2 bonds).

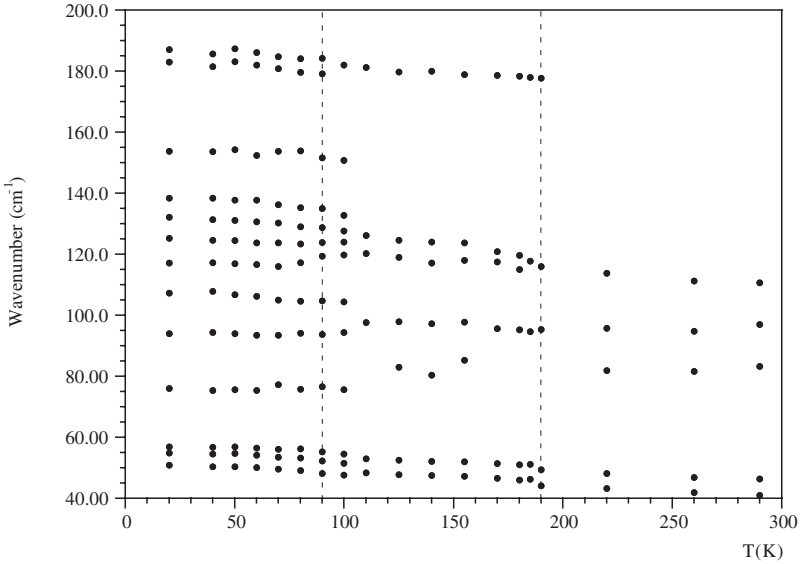

Figure 8. Temperature dependence of the frequencies of the fitted Raman spectra shown in figure 7. The vertical dashed lines mark the phase transition temperatures.

4.2. Temperature evolution of external modes

The temperature evolution of the Raman spectra below 220 cm^{-1} is shown in figure 7. At 190 K, most of the low-frequency spectra of the samples exhibit an abrupt and very strong decrease of intensity, especially in the $Y(ZY)X$ geometry, although some of the bands remain stable through this process. We were able to fit the spectra with seven independent damped harmonic oscillators (IDHO) in the temperature range RT–190 K. There is evidence for the existence of the betaine libration mode, at about 175 cm^{-1}, although it is impossible to fit it before T_{c1} is reached.

A splitting of most of these modes occurs below T_{c2} (figure 8). This splitting must be related to a breaking of the crystal symmetry at T_{c2}, where both rubidium and iodine ions lose their special positions permanently in the unit cell, and all modes acquire A symmetry and become Raman active.

The temperature dependence of the halfwidths ($\Delta\nu$) of some of these bands was also studied—most of these halfwidths exhibit a visible change of behaviour at T_{c2}. An Arrhenius-type function $\omega_r = A + B\exp(-E_a/k_BT)$ was fitted to the halfwidth versus temperature of the defined line at 96 cm^{-1} (the room temperature value) below T_{c2}, as described in the literature [16] (figure 9), with a calculated activation energy of $E_a = 0.019 \pm 0.002$ eV.

4.3. Internal modes

Water stretching vibrations ν_1^w and ν_3^w are found in the 3200–3600 cm^{-1} region of the Raman spectra [16], and the temperature evolution of this region of the spectra was studied in the $Y(ZZ)X$ geometry (figure 10). One can assume that water molecules are very weakly attached to the crystal lattice in the high-temperature phase, and therefore dynamically disordered. Hence, in the high-temperature phase their modes are very broad and overdamped. A gradual softening and narrowing of the bands on cooling is noticeable and there is an abrupt change

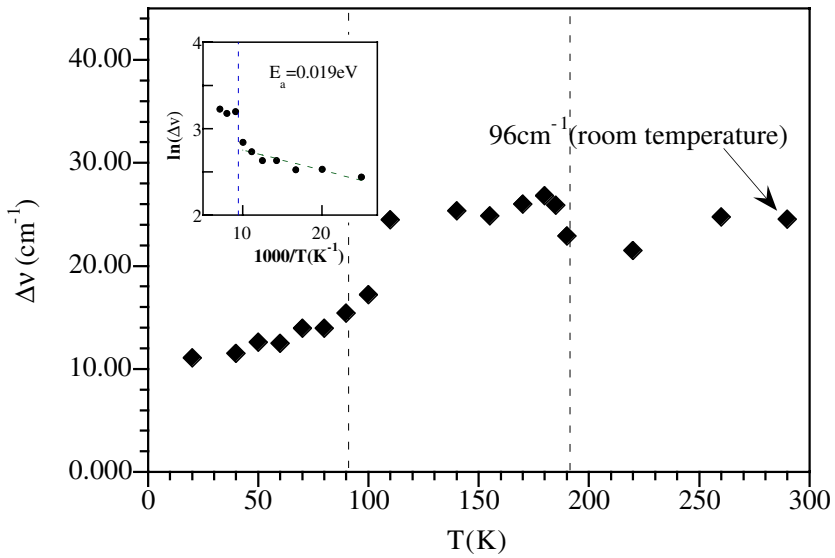

Figure 9. The temperature dependence of the halfwidth ($\Delta\nu$) of the well-defined band at 96 cm^{-1} (RT) in the $Y(ZY)X$ scattering geometry. The inset shows an Arrhenius plot of $\Delta\nu$ versus $1000/T$.

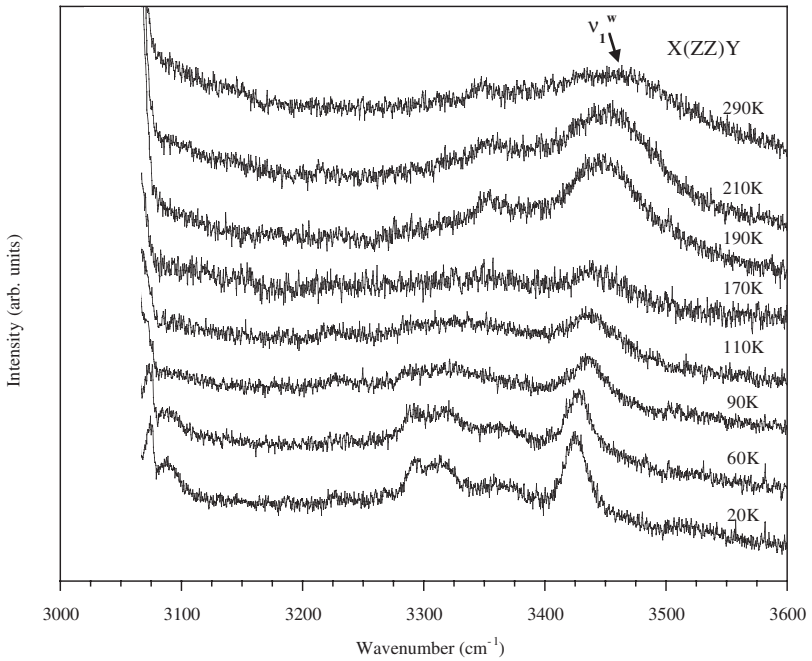

Figure 10. Temperature evolution of the Raman spectra in the region of O–H bonds and water molecule internal vibrations, for $Y(ZZ)X$ scattering geometry.

of intensities of some of the bands in this region of the spectra, at T_{c1} (figure 10). Other bands are also observed, assigned to the H-bond internal modes, expected in this region of the spectra [4].

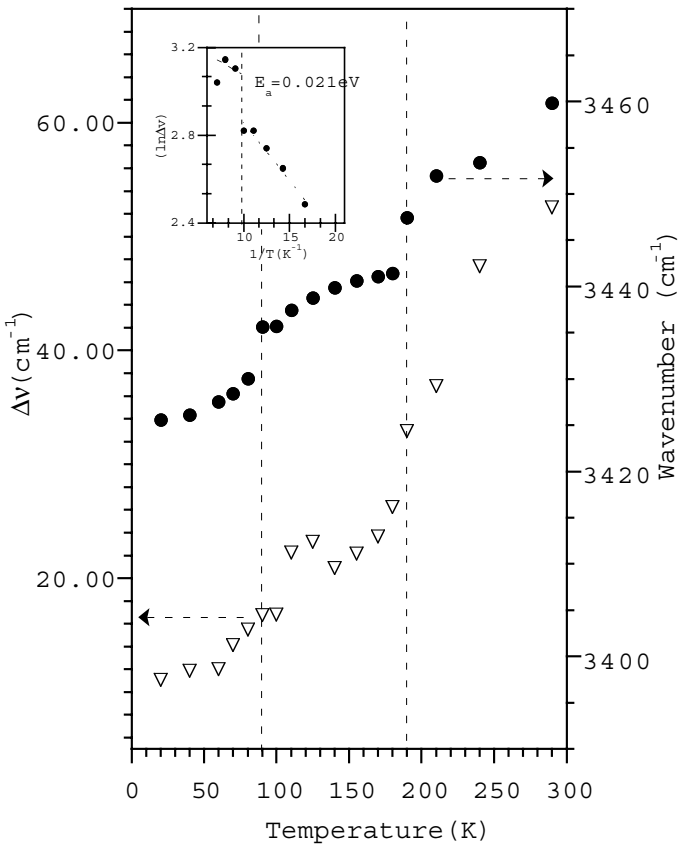

Figure 11. Temperature dependences of the halfwidth ($\Delta\nu$) and the frequency of the ν_1^w-band in the $Y(ZZ)X$ scattering geometry. The inset shows an Arrhenius plot of $\Delta\nu$ versus $1000/T$.

We assigned the band at 3460 cm^{-1} (room temperature) in $X(ZZ)Y$ geometry to a water stretching vibration mode ν_1^w. This mode shows a very interesting behaviour, gradually narrowing on cooling. It presents a dramatic frequency shift at T_{c1}, as well as near T_{c2}, of about 6 cm^{-1}. The halfwidth versus the temperature ($\Delta\nu(T)$) of this mode presents remarkable changes at the phase transitions (figure 11). An Arrhenius-type function, of the same type as the one described in section 4.2, was fitted to this halfwidth $\Delta\nu(T)$ in the 20–100 K range of temperatures. We calculated an activation energy of approximately 0.021 ± 0.002 eV, in close agreement with the value obtained in section 4.2. These values are of the same order of magnitude of the typical values observed for solid hydrates [16]. A small band appearing below T_{c2} at approximately 3520 cm^{-1} could be a second-order effect, although it could also be assigned to the water asymmetric stretching mode ν_3^w. This mode is not visible above T_{c2}.

We have assigned both bands at 3290 and 3370 cm^{-1} ($Y(ZZ)X$ geometry) to the internal vibrations of the C5–O2···H31 and O3–H32···O3 bonds. These bands split below T_{c2} corresponding to the creation of asymmetric H bonds. Besides, an additional broad band (at 3330 cm^{-1}) emerges at PT_2 giving evidence for a strong H bond between water molecules and the carboxyl group (O3–H31···O2). These bands are also observed in $Y(ZY)X$ geometry.

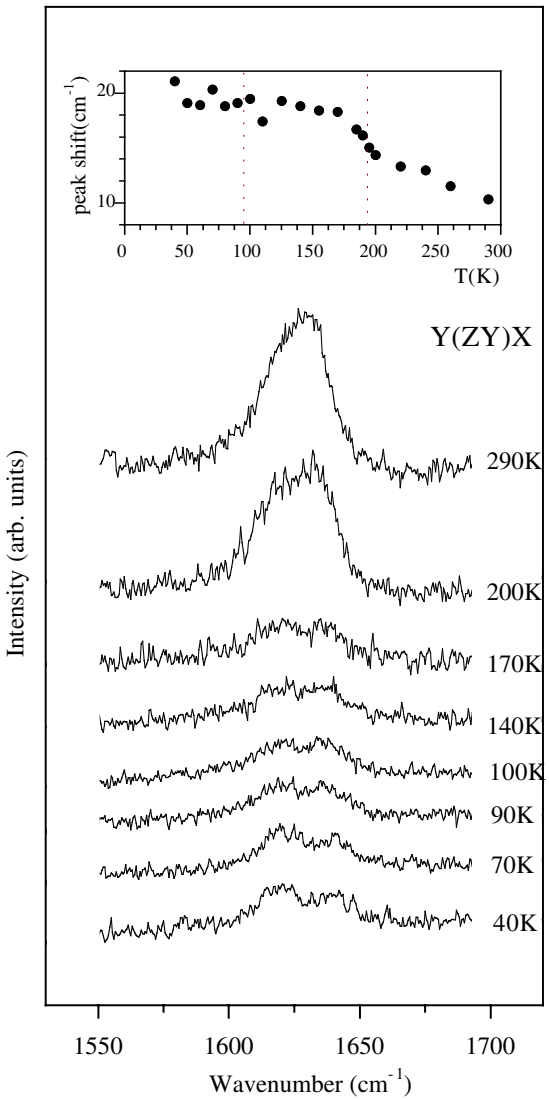

Figure 12. Temperature dependence of the Raman spectra in the region of the asymmetric vibrations of the carboxyl group, for $Y(ZY)X$ scattering geometry. The inset shows the peak shift of the fitted modes versus the temperature.

Three modes in the region 3040–3100 cm^{-1} have also been detected. It is still not very clear what their origin is. They might be associated with another H bond or with the methyl groups of the betaine. One of these bands splits in two smaller bands at T_{c2}. It must be noted that the frequencies of these peaks are rather stable throughout the temperature range.

As there is clear evidence for a strong bond between water molecules and the carboxyl group, as referred to above, the frequency range 1650–1750 cm^{-1} of the Raman spectra was investigated, where the asymmetric modes of the carboxyl group are usually found [17]. In fact, in the $Y(ZY)X$ geometry, two very close peaks were found in that region of the spectra, as can be seen in figure 12, and assigned to the carboxyl internal vibrations. The difference between

the maximum frequency of these two peaks (peak shift) versus the temperature, displayed in the inset of figure 12, increases on cooling, reflecting a more permanent bond of the water molecules to the crystal lattice.

5. Discussion and conclusions

As reported here, BRbI presents an interesting phase transition sequence from RT to 10 K. X-ray diffraction studies showed that water molecules are very weakly bond to each other at room temperature. The phase transitions observed at 190 and at 90 K are clearly related to water molecule reorientational degrees of freedom and to the dynamics of hydrogen bonds. The observed change of behaviour of $\omega_r(T)$ at $T_{c1} = 190$ K is clearly associated with the phase transition that occurs at this temperature. Water molecules lose most of their rotational energy due to a strengthening of their bond to the betaine molecules, as is shown by the peak shift observed in the Raman spectra of the carboxyl group internal modes. This phase transition is accompanied by an explicit change in the electrical conductivity of BRbI. The intense dc currents measured along the X- and Y-directions, above 190 K, are very probably due to proton conductivity along the zigzag chain of H bonds perpendicular to the c-axis, involving the water molecules and the carboxyl groups. This proton conductivity disappears below 190 K due to the strengthening of the H bonds in the crystal lattice.

The very dispersive relaxation process of the complex dielectric constant between 190 and 90 K shows that water molecules undergo a gradual freezing process. This process triggers, in this temperature range, a continuous and progressive slowing down of protonic fluctuations throughout the H-bond chains, until their permanent freezing in occurs at 90 K. This mechanism implies the existence of a proton-glass state at lower temperatures in BRbI. This glassy state is clearly supported by the absence of any induced polarization below 90 K, the β-values obtained (<1) and the non-existence of either simple or complex hysteresis loops, which excludes the possibility of ferroelectric or antiferroelectric behaviour.

In order to confirm the existence of a proton-glass state at low temperatures, additional experimental studies are necessary, for the determination of its structure in this temperature range. These studies are being undertaken and will be published elsewhere.

Acknowledgments

We are grateful to Dr J Albers for his collaboration in the study of betaine compounds. The authors thank A Costa for his technical assistance. This work was supported by the project POCTI/P/FIS/14287/98. Pedro Teles and Filipa Pinto thank POCTI/FIS/14287/98 and PRAXIS XXI for the grants BICJ/247847/2001 and BICJ/4688/96, respectively.

References

[1] Andrade L C R, Costa M M R, Paixão J A, Moreira J A, Almeida A, Chaves M R and Klöpperpieper A 1999 *Z. Kristallogr. NCS* **214** 83–4

[2] Andrade L C R, Costa M M R, Pinto F, Paixão J A, Almeida A, Chaves M R and Klöpperpieper A 2000 *Z. Kristallogr. NCS* **215** 537–8

[3] Yuzyuk Yu I, Almeida A, Pinto F, Chaves M R, Moreira J, Agostinho and Klöpperpieper A 2000 *J. Phys.: Condens. Matter* **12** 1497–506

[4] Yuzyuk Yu I, Almeida A, Chaves M R, Pinto F and Klöpperpieper A 2000 *J. Phys.: Condens. Matter* **12** 6253–64

[5] Andrade L C R, Costa M M R, Pinto F, Rodrigues V H, Paixão J A, Almeida A, Chaves M R and Klöpperpieper A 2001 *Z. Kristallogr. NCS* **216** 227–8
[6] Yuzyuk Yu I, Dmitriev V, Rabkin L, Burmistrova L, Shuvalov L, Smutný F, Vanek P, Gregora I and Petzelt J 1995 *Solid State Ion.* **77** 122–7
[7] Yuzyuk Yu I, Dmitriev V P, Rabkin L M, Gregora I, Smutný F and Shuvalov L A 1996 *Solid State Ion.* **91** 145–53
[8] Pirc R, Tadíc B and Blinc R 1992 *Physica* A **185** 322–30
[9] Banys J, Klimm C and Völtel G 1994 *Phys. Rev.* B **50** 16751–3
[10] Orešic M and Pirc R 1993 *Phys. Rev.* B **47** 2655–60
[11] Ries H, Böhmer R, Fehst I and Loidl A 1996 *Z. Phys.* B **99** 401–11
[12] Lopes dos Santos J M B, Santos M L, Chaves M R, Almeida A and Klöpperpieper A 2000 *Phys. Rev.* B **61** 8053
[13] Höchli U T, Knorr K and Loidl A *Adv. Phys.* **39** 405–615
[14] Chaves M R, Amaral M H and Ziolkiewiecz 1980 *J. Physique* **41** 259
[15] Gouda F M 1992 *PhD Thesis* Chalmers University of Technology, Götenburg
[16] Lutz H D 1988 *Struct. Bonding* **69** 99
[17] *Handbook of Chemistry and Physics* 1989 ed R C Weast (Boca Raton, FL: Chemical Rubber Company Press)